FIBER ASPECT RATIO CHARACTERIZATION AND STIFFNESS PREDICION IN LARGE-AREA, ADDITIVE MANUFACTURED, SHORT-FIBER COMPOSITES

Timothy Russell, David Jack
Baylor University

Abstract

Previously, the authors of this study developed a methodology for predicting the fiber orientation state and effective elastic modulus of a short-fiber, polymer composite bar fabricated using large-area additive manufacturing (LAAM). The predictions were made for a 13 wt% carbon fiber reinforced acrylonitrile butadiene styrene (ABS). Predicting the internal fiber orientation state of the sample and the elastic modulus (a function of the orientation state) requires knowledge of the fiber aspect ratio. Previously, the fiber aspect ratio was chosen arbitrarily, albeit within reason. In this study, we sought to experimentally characterize it and update our predictions. We found and present both the weighted average and the number average of the fiber aspect ratio of the 13 wt% carbon fiber ABS both before and after the material has been processed in the LAAM machine. We then use these aspect ratio values to make predictions of the fiber orientation state and the resulting elastic modulus of a tensile bar.

Background and Requirements

Composite materials and 3D printing technology both offer very attractive advantages to the manufacturing industry. Composite materials offer high strength- and stiffness-to-weight ratios and give engineers the ability to tailor parts to meet criteria for specific loading scenarios. 3D printing, also known as additive manufacturing, also has advantages. In most cases, 3D printing involves building a part from a CAD file in a layer-by-layer fashion based on many 2D print patterns laid up at increasing z-heights. This processing technique offers a designer the ability to design a part with little wasted material, add complexity to the part for free, and avoid the need for a mold, saving time and money.

Large area additive manufacturing (LAAM) of composite materials is where large scale manufacturing, additive manufacturing, and composite materials meet. However, in order for LAAM of short-fiber composites to be a dependable means of manufacturing parts, it is important to devise a method of predicting the processing effects on the final properties of a LAAM-made, short-fiber composite part. To predict these properties requires a method of first predicting the fiber orientation state within the processed part, since a non-random fiber orientation state would give the part anisotropic properties.

Predicting the fiber orientation state has been well researched when it comes to manufacturing short-fiber composites in the injection and compression molding industries but not in regards to 3D printing, specifically 3D printing of the polymer extrusion deposition variety like we investigate here. Predicting the fiber orientation state involves knowing the behavior of the polymer melt flow (the velocity profile), the shape of the fibers, and how the fibers interact with their surroundings. Traditionally, fiber orientation modeling is done with the flow and orientation state weakly coupled. That is, the flow affects the orientation state, but the orientation state is not allowed to affect the flow. (This is not actually true though since the flow viscosity is a function of the fiber orientation state.) In addition, inertial effects are neglected in fiber orientation modeling and the fibers are assumed to be rigid and of uniform distribution, shape, and aspect ratio. Generally, fiber interactions with walls are not taken into account.

However, fiber-to-fiber interaction is traditionally taken into account using a diffusion term to artificially randomize the fiber orientation state. Models that include this diffusion term are required for modeling concentrated fiber suspensions. Folgar and Tucker introduced the use of the diffusion term in their 1984 Isotropic Rotary Diffusion (IRD) model [1], based on Jeffrey's 1922 model for the motion of a single, rigid ellipsoidal fiber [2], and their model is commonly used in the injection molding industry [3]. However, the Reduced Strain Closure (RSC) model of 2008 by Wang *et al.* is more accurate at predicting the transient fiber orientation state [4]. The RSC model includes a parameter (κ) which slows down the rate at which the steady orientation state is achieved. Both κ in the RSC model and the fiber interaction term C_I, which is contained in the diffusion term and appears in both the IRD and RSC models, must be found empirically. We chose to use the RSC model in this study.

Furthermore, it is too computationally expensive to model the motion of every fiber in the processing of most short-fiber composite parts. Therefore, Advani's orientation tensors [5,6] are often used. These orientation tensors compactly describe the orientation state of a population of fibers [5,6] making the computation of the fiber orientation state feasible for concentrated fiber suspensions on today's computers. There are an infinite number of orientation tensors but the second- and fourth-order orientation tensors provide all of the orientation information needed to calculate second- and fourth-order tensor properties like stiffness, coefficient of thermal expansion, and conductivity [6]. The second- and fourth order tensors, respectively, are

$$\mathbf{A} = \oint \mathbf{pp}\psi(\mathbf{p})d\mathbf{p},\ \mathbb{A} = \oint \mathbf{pppp}\psi(\mathbf{p})d\mathbf{p} \tag{1}$$

where $\mathbf{p}$ is a unit vector designating the direction of a fiber, ψ is the fiber orientation probability density function, and the integrals are taken over all possible $\mathbf{p}$, which is the unit sphere.

Conveniently, the RSC model can be cast in terms of orientation tensors to describe the time rate of change of the orientation $\mathbf{A}$:

$$\begin{aligned}\frac{\mathrm{D}\mathbf{A}}{\mathrm{Dt}} = -\frac{1}{2}(\mathbf{\Omega}\cdot\mathbf{A} - \mathbf{A}\cdot\mathbf{\Omega}) + \frac{1}{2}\lambda\{\mathbf{\Gamma}\cdot\mathbf{A} + \mathbf{A}\cdot\mathbf{\Gamma} - 2\mathbf{\Gamma}[\mathbf{A_4} + (1-\kappa)(\mathbf{L_4} - \mathbf{M_4}:\mathbf{A_4})]\} \\ + 2\kappa C_I\dot{\gamma}(\mathbf{I} - 3\mathbf{A})\end{aligned} \tag{2}$$

In equation 2, $\mathbf{\Omega}$ and $\mathbf{\Gamma}$ are the vorticity and rate of deformation tensors, $\dot{\gamma}$ is the magnitude of $\mathbf{\Gamma}$, $\mathbf{L_4} = \sum_{i=1}^{3} n_i \boldsymbol{e}_i\boldsymbol{e}_i\boldsymbol{e}_i\boldsymbol{e}_i$, $\mathbf{M_4} = \sum_{i=1}^{3} \boldsymbol{e}_i\boldsymbol{e}_i\boldsymbol{e}_i\boldsymbol{e}_i$ for the eigenvalue n_i and eigenvector $\boldsymbol{e}_i$ of $\mathbf{A}$, and λ is a function of the fiber aspect ratio $a_r = length/diameter$. Technically,

$$\lambda = \frac{r_e^2 - 1}{r_e^2 + 1} \tag{3}$$

where r_e is the equivalent ellipsoidal aspect ratio, a function of a_r. The equivalent ellipsoidal aspect ratio for a cylindrical fiber such as the ones considered in this study can be expressed as

$$r_e = 0.000035a_r^3 - 0.00467a_r^2 + 0.764a_r + 0.404 \tag{4}$$

(see e.g. [7]). Thus, C_I, κ, and a_r are all parameters that must be experimentally characterized to properly model the fiber orientation in the processing of a short-fiber composite.

The fiber aspect ratio must also be known to predict the mechanical properties of the processed short-fiber composite. The micromechanics model of Tandon and Weng [8] is used in this study. Orientation homogenization is done on the transversely isotropic stiffness tensor provided by Tandon and Weng's model to get the stiffness tensor at any spatial point in the short-fiber composite. The homogenized stiffness tensor at a spatial point is given in terms of the orientation tensors at that point according to

$$\langle C_{ijkl}\rangle = b_1 A_{ijkl} + b_2\left(A_{ij}\delta_{kl} + A_{kl}\delta_{ij}\right) + b_3\left(A_{ik}\delta_{jl} + A_{il}\delta_{jk}\delta_{jl} + A_{jl}\delta_{ik}\delta_{jl} + A_{jk}\delta_{il}\right) + b_4\left(\delta_{ij}\delta_{kl}\right) + b_5(\delta_{ik}\delta_{jl} + \delta_{il}\delta_{jk}) \quad (5)$$

(see e.g. [6]) where $b_1 = \overline{C}_{1111} + \overline{C}_{2222} - 2\overline{C}_{1122} - 4\overline{C}_{1212}$, $b_2 = \overline{C}_{1122} - \overline{C}_{2233}$, $b_3 = \overline{C}_{1212} + 0.5(\overline{C}_{2233} - 2\overline{C}_{2222})$, $b_4 = \overline{C}_{2233}$, and $b_5 = 0.5(\overline{C}_{2222} + \overline{C}_{2233})$ and the $\overline{C}_{ijkl}$ values are the (i, j, k, l) components of the transversely isotropic stiffness tensor calculated with Tandon and Weng's micromechanics model.

Previously, the authors developed a methodology for predicting the bulk elastic modulus in the print direction of LAAM-made, short-fiber composite parts using the orientation tensor form of the IRD and RSC models [9–11]. The parameters C_I, κ, and a_r were chosen arbitrarily though and we know that these will affect the fiber orientation state prediction and through that, affect the elastic modulus prediction as well. The aspect ratio will also affect the bulk elastic modulus prediction through the micromechanics model itself. Actually, it has been shown that a_r can have a large impact on the elastic modulus prediction (see e.g. Wang *et al.* [12]), which is why accurate characterization of a_r is so important. Therefore, we seek to update our methodology for predicting the fiber orientation state and the bulk elastic modulus by experimentally characterizing a_r both before and after the 3D printing process. The material under consideration is a 13 wt% (8.38 vol%) carbon fiber filled ABS from PolyOne, whose constituent properties are given in Table ???.

Table I: Short-Fiber Composite Constituent Material Properties.

ABS Matrix Properties	Carbon Fiber Properties
$E_{ABS} = 2.25\ GPa$	$E_{CF} = 230\ GPa$
$\nu_{ABS} = 0.35$	$\nu_{CF} = 0.2$
$\rho_{ABS} = 1040\ kg/m^3$	$\rho_{CF} = 1700\ kg/m^3$

Computational Methods Used in this Study

The fiber orientation methodology used in this study matches that used previously in [9–11], although some of the boundary conditions in the flow model were updated in [11] and maintained for this study to match the physical 3D printer settings used when samples were 3D printed. First, it was necessary to calculate the velocity profile within the 3D printer extruder. This was done as a 2D, finite element model in COMSOL Multiphysics (Version 5.4; COMSOL Inc., Stockholm, Sweden, 2019). The entire flow geometry contains the tip of the 3D printer nozzle (whose dimensions are based on the actual Strangpresse Extruder Model 19 which is part of Baylor's LAAM system), the polymer melt die-swell, and the deposition of the printed polymer bead. This is shown in Figure 1 along with the boundary conditions of the problem. The geometry of the flow domain comes from Blake Heller of Baylor University and was generated according to his method of optimizing the shape of the die-swell (see e.g. Heller *et al.* [13,14]). This is the same geometry used in [9–11].

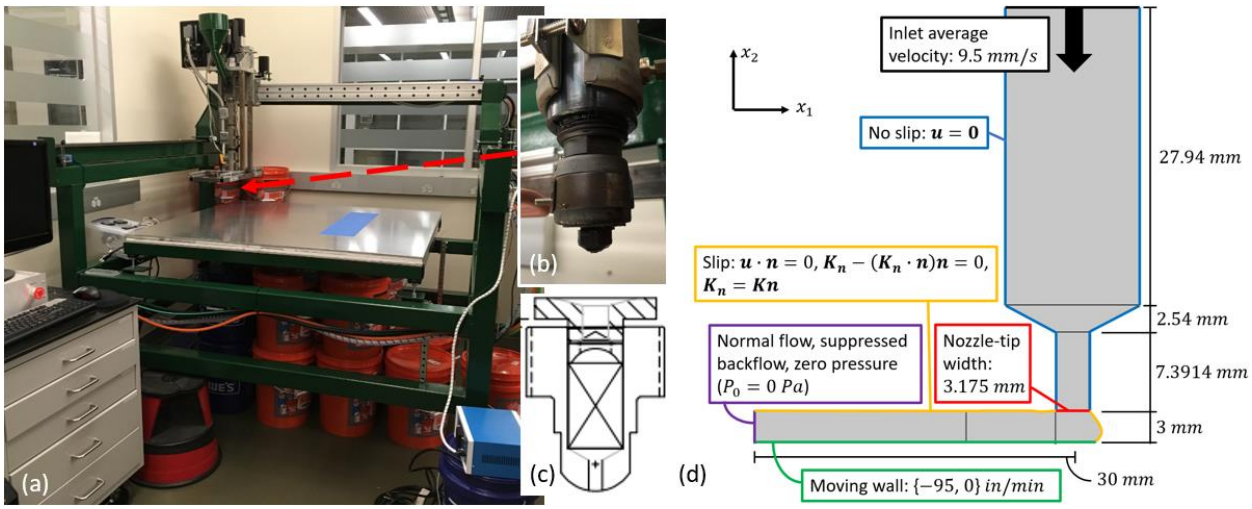

Figure 1. (a) Baylors LAAM system. (b) Close-up of nozzle. (c) Nozzle geometry. (d) COMSOL flow model.

Once the velocity field was found within the nozzle flow, the fiber orientation state was predicted as a function of that velocity field. The orientation state was predicted with the RSC model (equation 2), which was programmed along with equation 5 for the homogenized stiffness tensor in custom MATLAB (R2019a; MathWorks, 2019) codes. Using these codes, the homogenized stiffness tensor was predicted through the thickness (the x_2 dimension) of the printed bead. Then another COMSOL finite element model of a tensile sample was used to simulate tensile tests. The tensile sample was made up of 6 identical printed beads (2 beads wide, 3 beads tall) each with the same stiffness tensor properties. The dimensions of the tensile sample along with the boundary conditions of the tensile test simulations are shown in Figure 2. Only a thin, cross-sectional slice of a tensile bar is considered since the length of the sample has no effect on the predicted bulk elastic modulus and computational time is conserved this way. The width and height (the x_3 and x_2 dimensions) are based on actual tensile bars that were printed for a previous project in which it was found that rectangular shaped beads were a reasonable approximation to the actual bead geometry [11]. The entire front face of the tensile sample was given a prescribed displacement in the $-x_1$ direction, while the back face was fixed in the x_1 direction, fixed in the x_2 direction at the bottom left corner (to prevent rotation), and fixed in all directions at the bottom center. The bulk elastic modulus in the print direction of the tensile sample was derived after performing the tensile simulations.

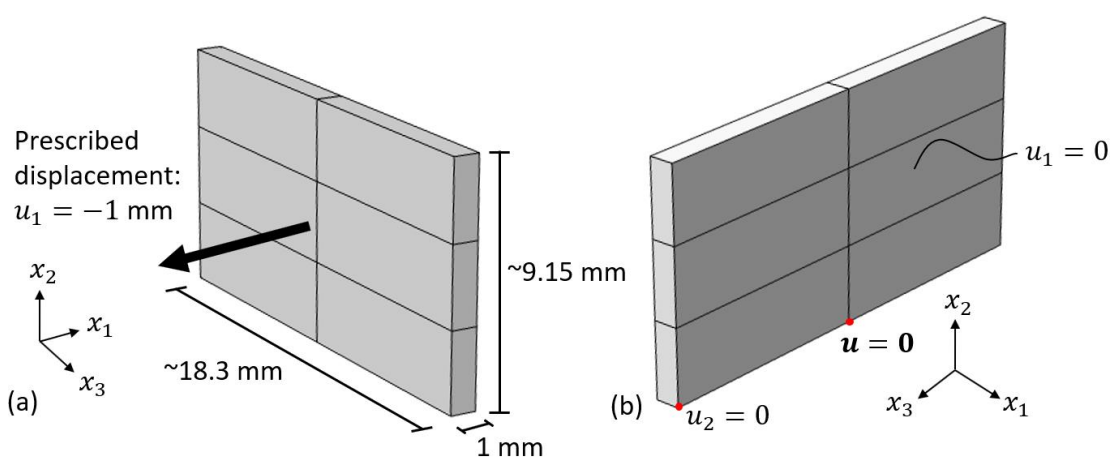

Figure 2. COMSOL tensile sample geometry and boundary conditions.

Experimentation

The fibers had to be isolated from the matrix of the composite before their lengths and diameters could be measured to get a_r. Burn-off tests are a valid method of doing this, so we performed burn-off tests of a pellet and a printed sample of the 13 wt% carbon fiber filled ABS. After the burn-off tests, fiber lengths and diameters were measured using microscopy.

Burn-off Testing

The pellet burn-off test was done in a TA Instruments Q50 Thermogravimetric Analyzer (TGA) machine which is pictured in Figure 3(a). The burn-off test in the TGA consisted of the following: (1) 20°C/min ramp up to 600°C in nitrogen, (2) isothermal for 1 hour in nitrogen, and (3) isothermal for 5 minutes in air. After several trial tests, it was found that the fibers tended to stay clumped together probably due to remnants of the ABS matrix. An early attempt at overcoming this issue was to soak the burn-off sample in acetone after the test to get rid of any remaining matrix. Acetone is known to corrode ABS and is often used to treat 3D printed, ABS parts to remove their rough surface texture, but it did not help us with separating the fibers as quickly as we had hoped. Boiling the acetone with the sample submerged in it did not help much either. Thus, we opted to include step (3) in our procedure and finish our burn-off tests with a non-inert air environment. Since carbon fiber will degrade in air at 600°C, we let step (3) only last for 5 minutes. Figure 3(b) shows a typical pellet and Figure 3(c) shows data from our burn-off test of the pellet. The final value of the wt% was 8%, a little lower than the nominal 13 wt%, so we probably let the pellet burn too long in the air. However, a 1-minute burn time in air was not long enough to be able to separate the fibers easily afterwards. Due to time constraints on this project, we decided to proceed with the pellet that had been burned for 5 minutes in air.

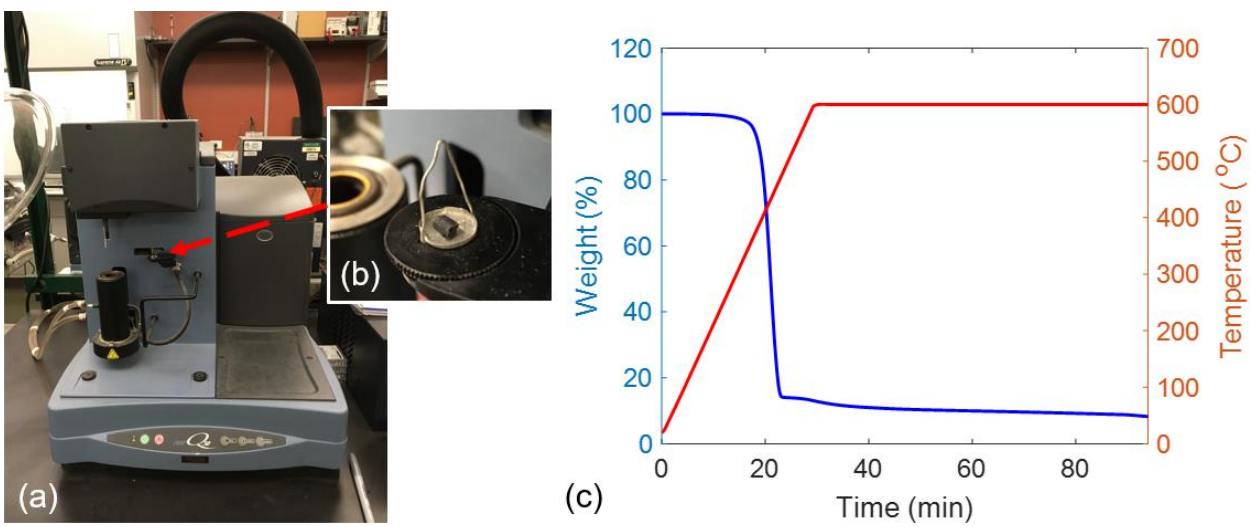

Figure 3. (a) TA Instruments TGA machine. (b) Typical pellet. (c) Plot of TGA burn-off test data.

For the burn-off test of the 3D printed sample, singular beads were printed at 210°C on an 85°C heated print bed. (For additional details on how Baylor's LAAM system is operated the reader is referred to the authors' early work [11].) After the beads were printed, the burn-off sample was cut from a bead. Cutting the bead, however, involves probable cutting of fibers and, hence, an erroneous measurement of the fiber length distribution (FLD). Therefore, to help minimize the effect that cut fibers would have on the FLD, a "long," 2 inch sample was cut from the printed bead. This was much longer than the average pellet length which was determined to be about 0.16 inches after measuring 20 pellets. The average pellet length corresponds to the length of the longest fibers, so any fibers that might be cut would lay in the hashed areas of the

sample shown in Figure 4. The fibers that would not be at risk of being cut would lay in the solid black region of the sample in Figure 4, which makes up about 84% of the entire sample.

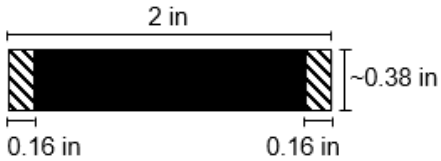

Figure 4. Dimensions of the 3D printed sample to be burned off.

The dimensions of the 3D printed sample were unfortunately too large for the sample to fit into the TGA. However, the sample still needed to be burned off in nitrogen, so the test setup shown in Figure 5(a) was made. A Ney Vulcan 3-1750 box furnace was used, and the sample was contained in a petri dish with an aluminum lid as shown in Figure 5 (b). The lid was milled to fit the petri dish and two holes were drilled and tapped on top of the lid to allow two steel tubes to be connected to it. The steel tubes were fit through the vent at the top of the furnace and carried nitrogen (N) in and out of the sample container. A gas bubbler was attached at the end of the outgoing nitrogen tube to prevent air from backflowing into the sample container during the test. A similar procedure as was used for the TGA test was used for this burn-off test: (1) 20°C/min ramp up to 600°C, (2) isothermal for 1 hour in nitrogen, and (3) isothermal for 10 minutes in air. Since the printed sample, shown after burn-off in Figure 5(c), was much bigger than a pellet, step (3) was done for 10 minutes rather than 5 to help free the carbon fibers.

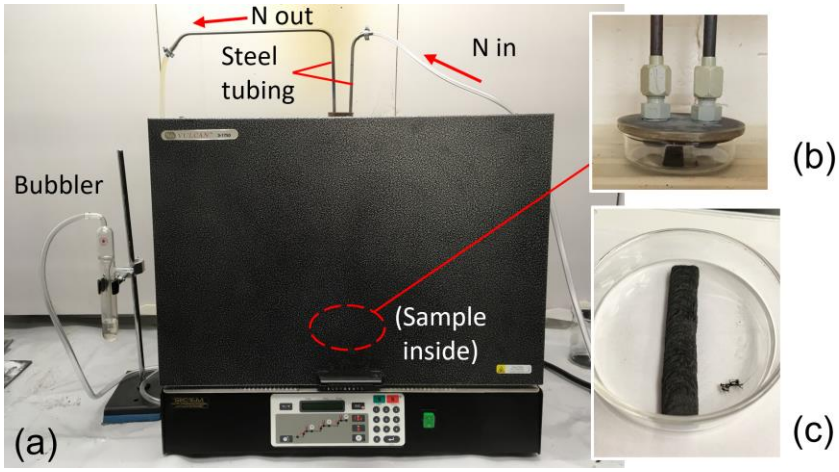

Figure 5. Bead burn-off test setup.

After the burn-off tests of the pellet and 3D printed sample, the burn-off samples were dropped into beakers of acetone and sonicated in the acetone with a Branson Digital Sonifier 450 (see Figure 6(a)) to disperse the fibers without damaging them. Sonication was typically done at 20% for no more than a few minutes. Sharma *et al.* found that after sonicating a long fiber thermoplastic burn-off sample in water and pouring the water-fiber solution into several petri dishes, one could choose any petri dish at random for the FLD measurements and it was of little consequence [15]. Therefore, immediately after the fibers were sonicated in the acetone and before they sank, a small amount of fiber-acetone solution was poured into a petri dish or multiple petri dishes and only one petri dish was selected to be used for FLD measurements. Only a small amount of fiber-acetone solution was poured into a petri dish because the fibers needed to be well dispersed so that they could be easily identified and measured under a

microscope. In addition, it was advantageous to use acetone for this part of the experiment because it dried quickly. Figure 6(b) shows the fibers dispersed in a petri dish after sonication (they are very small).

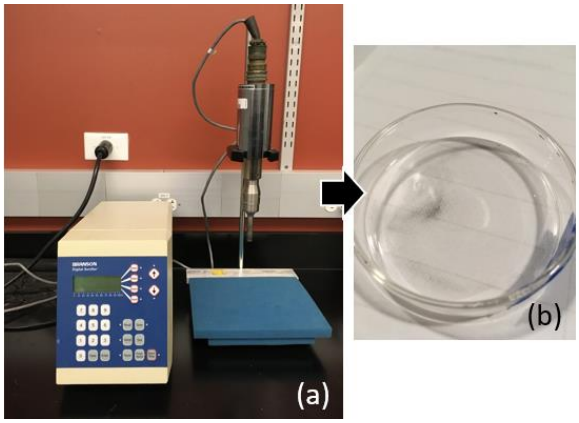

Figure 6. (a) Digital sonifier and (b) Fibers in a petri dish, ready to measure.

Measuring Fiber Lengths and Diameters

The fiber lengths were measured with a Keyence VR-3000 One-shot 3D Measurement Macroscope pictured in Figure 7. This system is connected to a computer on which a user can view his sample. Fiber lengths are measured by performing two mouse clicks on either end of a fiber. Figure 7 shows an example of what this looks like. The Keyence software allows one to stitch together multiple images to create a large image that is at a high magnification. The user is limited to being able to stitch together 100 images, however, so in order to photograph the whole petri dish, a magnification of only 25x was used. The fibers can still be seen fairly clearly but the resolution is not great and it can be difficult to identify the ends of fibers when they are overlapping each other as one can see in the circled parts of Figure 8. Not correctly identifying the ends of overlapping fibers undoubtedly contributed to measurement error during this part of the experiment although it is difficult to quantify how much. In the future, instead of being limited by the Keyence software's stitching abilities, we would like to capture images with the Keyence at a much higher magnification and stitch together the images using MATLAB or Adobe Photoshop. This has been a first pass experiment at measuring the FLD, so we expect our methods to improve considerably in time.

Figure 7. Keyence VR-3000 One-shot 3D Measurement Macroscope .

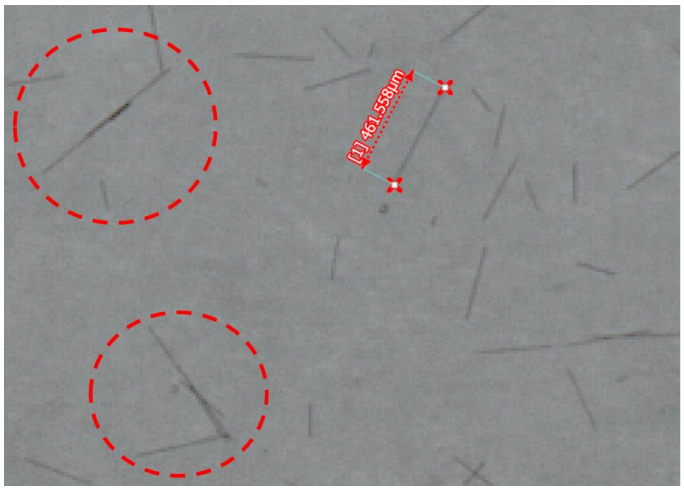

Figure 8. Keyence imaging and fiber length measuring.

Sharma *et al.* discovered that for long-fiber thermoplastic composites a sample size of 800 fibers would yield a number-average and a weight-average length that were less than 5% different from the number-average and weight-average length of a sample size of 2000 fibers [15]. Thus, 800 fibers were measured for both the pellet burn-off sample and the 3D printed burn-off sample. The FLDs for both samples are given in Figure 8. The number-average length L_n and weight-average length L_w, which are also shown in Figure 8, are calculated according to the equations (see e.g. [15])

$$L_n = \frac{\sum N_i L_i}{\sum N_i} \tag{6}$$

$$L_w = \frac{\sum N_i L_i^2}{\sum N_i L_i} \tag{7}$$

As one can see, the fiber lengths are shorter for the 3D printed sample indicating that fiber breakage has happened during processing. The distribution is not a clear Weibull distribution, as might be expected, probably due to human error during the fiber measurements.

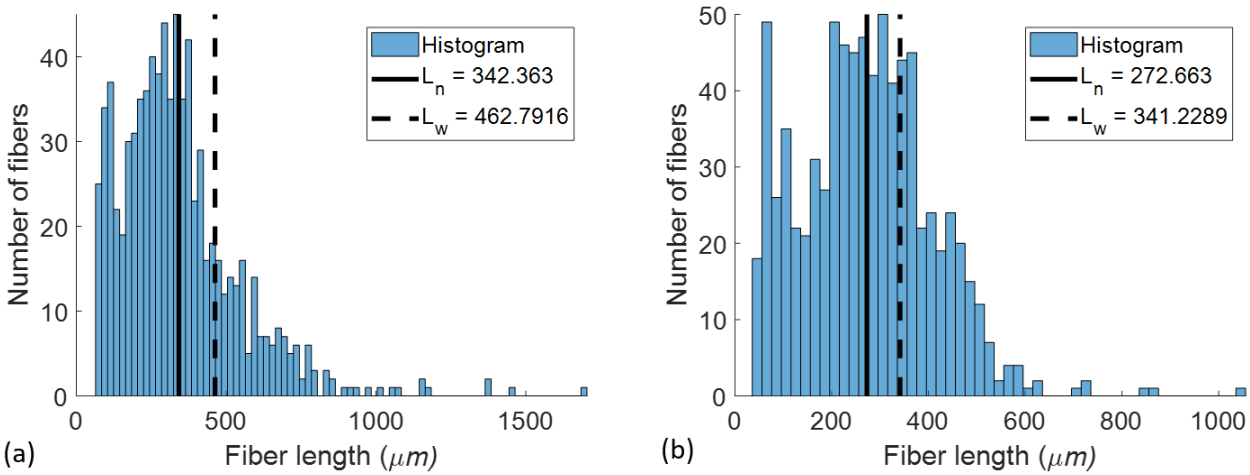

Figure 9. FLD of (a) pellet and (b) bead.

To measure the fiber diameters, a higher magnification was required. Thus, a JEOL JSM-6610LV Scanning Electron Microscope (SEM), pictured in Figure 9, was used for measuring the fiber diameters. Typical fiber diameter measurements are shown in Figure 10 at a magnification of 1100x.

Figure 10. JEOL JSM-6610LV Scanning Electron Microscope.

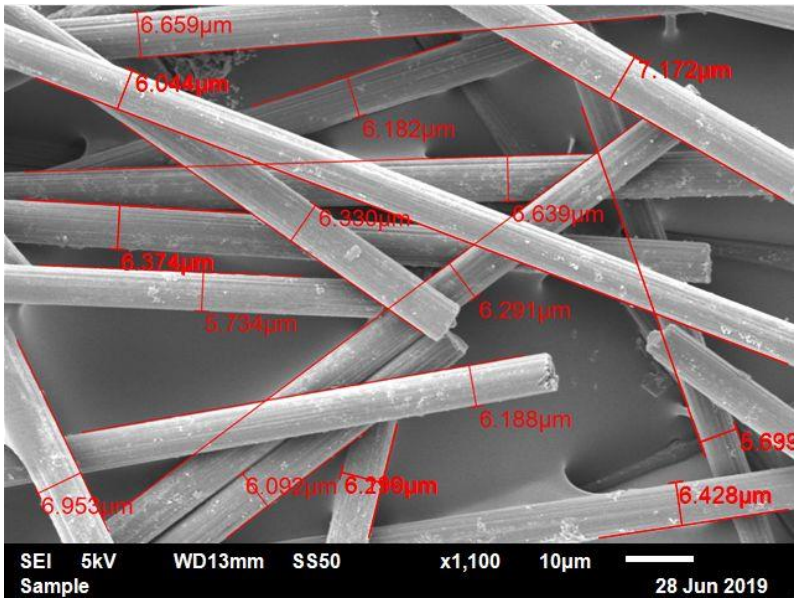

Figure 11. SEM imaging and fiber diameter measuring.

Results

Table 2 summarizes the fiber length and diameter measurements. The mean fiber diameter μ_d was found from 14 fiber diameter measurements for the pellet fibers and from 24 for the bead fibers. The standard deviation for the fiber diameters is small, so the number-average and weight-average fiber aspect ratios, $a_{r,n}$ and $a_{r,w}$, were found by dividing the L_n and L_w values by the μ_d values. Technically, the true $a_{r,n}$ and $a_{r,w}$ would require all of the length and diameter measurements to be made for exact same fibers, but it was unfeasible to measure the lengths of 800 fibers using the SEM or to measure fiber diameters with the Keyence machine. One may notice from the table that fiber diameters for the 3D printed bead are smaller on average than those of the pellet. This is likely due to the fact that there was a 10 minute burn in air during the burn-off test of the printed bead.

Table 2: Results Summary.

	Pellet	3D Printed Bead
L_n	$342.36\ \mu m$	$272.66\ \mu m$
L_w	$462.79\ \mu m$	$341.23\ \mu m$
μ_d	$6.93\ \mu m$	$6.37\ \mu m$
σ_d	$0.36\ \mu m$	$0.39\ \mu m$
$a_{r,n}$	49.39	42.82
$a_{r,w}$	66.85	53.59

Once the weight-average fiber aspect ratios were determined, the computation of the effective, bulk, elastic modulus in the print direction of a tensile sample was carried out according the methods outlined earlier. Figure 12 shows effective E_{11} predictions for several

different aspect ratios. One can see that the predictions increase with increasing aspect ratio and our updated aspect ratio makes a tremendous difference. As it stands now, the best aspect ratio for us to use for our future modeling would be $a_{r,w} = 53.593$ from the 3D printed bead.

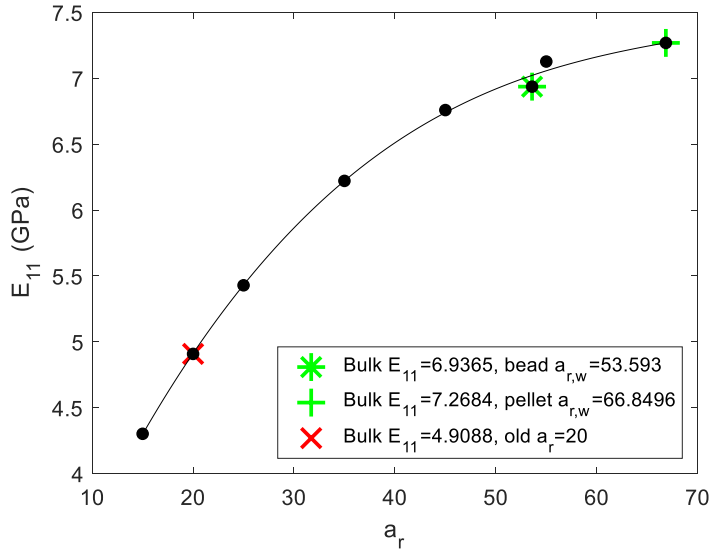

Figure 12. Effective elastic modulus as a function of a_r. (Used RSC with $C_I = 0.01$, $\kappa = 0.11$).

Summary and Next Steps

This was a preliminary study on measuring the fiber aspect ratio in 13 wt% carbon fiber filled, large volume, 3D printed samples. Our burn-off tests and imaging techniques need to be further refined in order to more accurately measure the fiber aspect ratio, but we now know that we were previously using an aspect ratio that was much too low for our predictions of the bulk, effective, elastic modulus in the print direction of a 3D printed sample.

Acknowledgements

Thanks goes to Blake Heller and Dr. Douglas Smith for permitting the use of their nozzle geometry for flow model as well as Baylor University for funding this project. Thanks to Daniel Pulipati and Rifat Nargis for help in the imaging portion of this project as well.

Bibliography

[1] Folgar, F., and Tucker, C. L., 1984, “Orientation Behavior of Fibers in Concentrated Suspensions,” Journal of Reinforced Plastics and Composites, **3**(2), pp. 98–119.

[2] Jeffery George Barker, and Filon Louis Napoleon George, 1922, “The Motion of Ellipsoidal Particles Immersed in a Viscous Fluid,” Proceedings of the Royal Society of London. Series A, Containing Papers of a Mathematical and Physical Character, **102**(715), pp. 161–179.

[3] Phelps, J. H., and Tucker, C. L., 2009, “An Anisotropic Rotary Diffusion Model for Fiber Orientation in Short- and Long-Fiber Thermoplastics,” Journal of Non-Newtonian Fluid Mechanics, **156**(3), pp. 165–176.

[4] Wang, J., O’Gara, J. F., and Tucker, C. L., 2008, “An Objective Model for Slow Orientation Kinetics in Concentrated Fiber Suspensions: Theory and Rheological Evidence,” Journal of Rheology, **52**(5), pp. 1179–1200.

[5] Advani, S., 1987, “Prediction of Fiber Orientation during Processing of Short Fiber Composites,” ProQuest Dissertations Publishing.

[6] Advani, S. G., and Tucker, C. L., 1987, “The Use of Tensors to Describe and Predict Fiber

Orientation in Short Fiber Composites," Journal of Rheology, **31**(8), pp. 751–784.
[7] Zhang, D., E. Smith, D., A. Jack, D., and Montgomery-Smith, S., 2011, "Numerical Evaluation of Single Fiber Motion for Short-Fiber-Reinforced Composite Materials Processing," J. Manuf. Sci. Eng, **133**(5), pp. 051002-051002–9.
[8] Tandon, G. P., and Weng, G. J., 1984, "The Effect of Aspect Ratio of Inclusions on the Elastic Properties of Unidirectionally Aligned Composites," Polymer Composites, **5**(4), pp. 327–333.
[9] Russell, T., Heller, B., Jack, D. A., and Smith, D. E., 2018, "Prediction of the Fiber Orientation State and the Resulting Structural and Thermal Properties of Fiber Reinforced Additive Manufactured Composites Fabricated Using the Big Area Additive Manufacturing Process," Journal of Composites Science, **2**(2), p. 26.
[10] "Russell_Initial Fiber Orient Effects to Predict T-M Props of Large Volume, Fused Filament Comps_AM3D.Pdf," Dropbox [Online]. Available: https://www.dropbox.com/s/hob0d27jeouodst/Russell_Initial%20Fiber%20Orient%20Effects%20to%20Predict%20T-M%20Props%20of%20Large%20Volume%2C%20Fused%20Filament%20Comps_AM3D.pdf?dl=0. [Accessed: 27-Jun-2019].
[11] Russell, T., and Jack, D., 2019, "Stiffness Prediction and Validation of Large Volume 3D Printed, Short-Fiber-Filled Polymer Composites."
[12] Wang, Z., E. Smith, D., and A. Jack, D., 2018, "Effects of Fiber Aspect Ratio on Predicted Elastic Properties of Short Fiber Reinforced Composites Printed by Large Scale Polymer Additive Manufacturing."
[13] Heller, B. P., Smith, D. E., and Jack, D. A., 2016, "Effects of Extrudate Swell and Nozzle Geometry on Fiber Orientation in Fused Filament Fabrication Nozzle Flow," Additive Manufacturing, **12**, pp. 252–264.
[14] Heller, B. P., Smith, D. E., and Jack, D. A., "SIMULATION OF PLANAR DEPOSITION POLYMER MELT FLOW AND FIBER ORIENTAITON IN FUSED FILAMENT FABRICATION," p. 16.
[15] Sharma, B. N., Kijewski, S. A., Fifield, L. S., Shin, Y., Tucker, C. L., and Sangid, M. D., 2018, "Reliability in the Characterization of Fiber Length Distributions of Injection Molded Long Carbon Fiber Composites," Polymer Composites, **39**(12), pp. 4594–4604.